Malaysian Journal of Chemistry, 2026, Vol. 28(1), 501-513
(Special Issue: *12th International Conference of the College of Science & 3rd Conference of Chemistry Department 2025*)

Photochemical Synthesis and Adsorptive Efficiency of NiS–SrO Nanostructures for Tartrazine Dye Removal from Wastewater

Sara Younis Abdullah and Ahmed Mahdi Rheima*
Chemistry Department, Mustansiriyah University College of Science, Baghdad, 10011, Iraq
*Corresponding author (e-mail: ahmed.rheima@gmail.com)

Industrial food dyes are one of the chemical pollutants in the aquatic environment. They are released with food wastewater, altering the physical and chemical properties of the water, directly impacting living organisms and humans. In this study, a novel photochemical technique utilizing ultraviolet light was employed to produce binary NiS–SrO nanoparticles. While TEM investigation showed the development of nearly spherical nanoparticles with an average diameter of 22 nm, structural characterization using XRD confirmed the composite's crystalline structure, with crystallite sizes of 18.7 nm. FE-SEM analyses revealed a very porous surface shape, which is beneficial for adsorption processes. In demonstrating that nickel, sulfur, strontium, and oxygen were evenly distributed throughout the nanocomposite, elemental mapping and EDX investigations further confirmed the successful creation of the intended binary material. Additionally, the ability of the produced NiS-SrO nanoparticles was their ability to adsorb impurities of tartrazine dye in aqueous solutions. The adsorption tests demonstrated that the binary nanomaterial outperformed its single-component counterparts in terms of dye removal effectiveness. The process is endothermic and spontaneous, as indicated by the positive ΔH° and negative ΔG° readings, and the adsorption capacity increased with temperature. The evaluation indicates that the adsorption follows a pseudo-second-order kinetic model, pointing to physisorption as the mechanism for capturing dye molecules. Putting the results together, the data portray NiS–SrO nanoparticles as a choice for extracting colorants from wastewater, thanks to their distinctive adsorption capacity and advantageous structural traits.

Keywords: NiS–SrO Nanoparticles, Tartrazine yellow dye, Adsorption study, photolytic synthesis, isotherm model, kinetic study, structural characterization

Received: October 2025; Accepted: October 2025

Pollutant water contamination has surged into the limelight of concerns in recent years [1]. Though a multitude of sources feed the crisis, organic dyes emerge as the agents that profoundly impair ecosystem vitality [2]. A million tons of these compounds are synthesized each year across the globe, feeding the appetites of the food, cosmetics, textile, and pharmaceutical sectors, alongside workshops, sprawling factories, and tanneries alike [3]. Their stubborn persistence derives from architectures that confer remarkable stability [4]. Alas, these colorants are toxic, imperiling both fauna and flora and diminishing the charm of watercourses [5]. Dyes can alter the behavior of aquatic plants during photosynthetic processes because they decrease light penetration [6]. Furthermore, many aquatic creatures can develop cancer as a result of exposure to certain toxic dyes [7].

Additionally, because of the emergence of numerous illnesses, pathologies, and syndromes, these dyes have been recognized as hazards to human health [8]. The food, textile, and dyeing industries utilize tartrazine extensively, and the fact that it persists in wastewater poses serious health and environmental issues [9]. Thus, creating effective, affordable, and environmentally friendly adsorbents is essential for long-term water purification initiatives [10]. Consequently, devising ways to strip dyes from wastewater has become a pursuit [11]. In this arena, nanotechnology opens pathways through engineering. Finely tuning nanomaterials to their surface area, these nanomaterials can seize dye molecules sharply, lowering concentrations and easing toxicity concerns [12, 13]. Nanorods, nanoparticles, and nanotubes are typical examples [14]. SrO-NiS-based nanocomposites have been the focus of recent studies and have been praised for their multifunctional performance, vigorous activity, and high removal efficiency [15, 16]. The main benefits of choosing synthesis pathways are a reduced energy footprint and the avoidance of harsh reagents [17, 18]. In light of this, the current work describes the production and comprehensive characterization of NiS–SrO nanoparticles, examining their capacity to adsorb the color tartrazine from media [19]. Temperature, contact time, and other comparable parameters are among the operating settings in which its adsorption capacity is examined to shed light on the underlying mechanisms [20, 22]. In the beginning, NiS-SrO nanoparticles were created,

†Paper presented at the 12th International Conference of the College of Science & 3rd Conference of Chemistry Dept. 2025

and their ability to remove Tartrazine color from the media was then assessed. To determine whether the composite could be used to treat wastewater, the researchers tested its adsorption capacity. Determined the governing parameters for the uptake.

EXPERIMENTAL

Synthesis of Binary NiS –SrO Nanoparticles

All materials used in this project are of high purity and prepared from Sigma Aldrich and were used without any impurity. A dedicated photolysis rig performed the synthesis. To guarantee that UV photons could pass through the reaction mixture unhindered, the setup included a cell chosen for its transmission of UV light. As illustrated in Figure 1, a Pyrex tube served as the main reaction vessel. To prevent excessive heating from UV exposure, the reactor was kept in an ice bath (under -5 °C) throughout the process. Illumination was provided by a 125 W medium-pressure mercury lamp, delivering maximum intensity at a wavelength of 365 nm. The binary NiS-SrO NPs were created by a series of steps. To establish a uniform suspension, 1.0 g of SrO powder was dispersed in 100 mL of de-ionized water (D.W.) and constantly agitated. The suspension was gradually exposed to 100 mL of 20 Mm nickel nitrate solution (Ni $(NO_3)_2$) at a rate of one drop per second. Then, 50 ml of 20 Mm urea was added slowly with stirring. After being obtained, the product was placed into the photochemical reactor and exposed to UV light for thirty minutes. After this was completed, a 100 Mm sodium sulfide (sulfur source) solution was added, which caused black powder to develop immediately. The necessary NiS–SrO nanoparticles were obtained by carefully collecting the solid product, repeatedly washing it with D.W. to remove any remaining ions, and then drying it in an oven set at 90 °C for five hours.

Adsorption Study

Adsorption experiments were conducted in batch mode to evaluate the removal of Tartrazine dye with NiS-SrO nanoparticles. In every experiment, 10 mg of nanoparticles were added to 10 mL of Tartrazine yellow dye solutions at varied concentrations (5, 10, 15, 20, and 25 ppm). The mixes were shaken in a thermostatic water bath shaker at controlled speeds, temperatures, and contact times. Following equilibration, the suspensions were centrifuged at 3500 rpm for 5 minutes to separate the supernatant. The concentration of leftover dye was evaluated using UV-Vis spectrophotometry at a maximal absorbance wavelength of 425 nm. The adsorption efficiency (R %) and equilibrium adsorption capacity (q_e) were estimated using the following equations [21]:

$$R\% = 100 \times (C_i - C_e) / C_i \quad (1)$$

$$q_e = V (C_i - C_e) / m \quad (2)$$

Where q_e (mg/g) represents the adsorption capacity at equilibrium, C_i and C_e (mg/L) are the initial and equilibrium dye concentrations, V is the solution volume (L), and m is the mass of SrO–NiS nanoparticles (g) [22]. Chemicals and materials chemicals and materials.

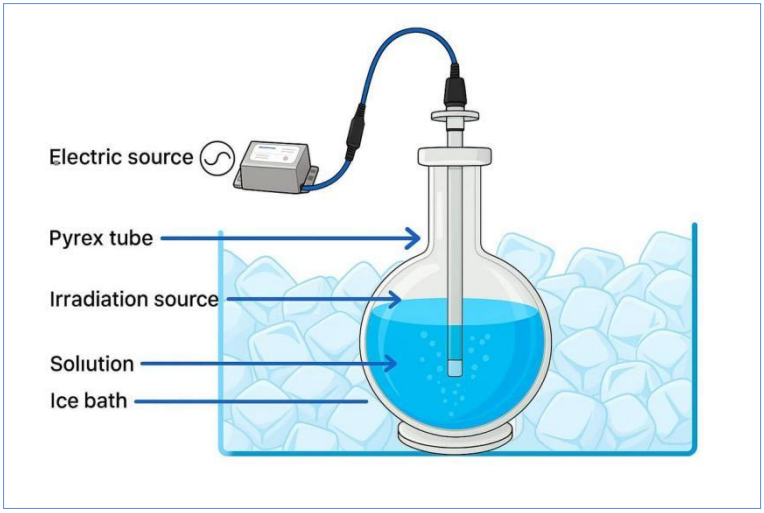

Figure 1. Photolysis Cell.

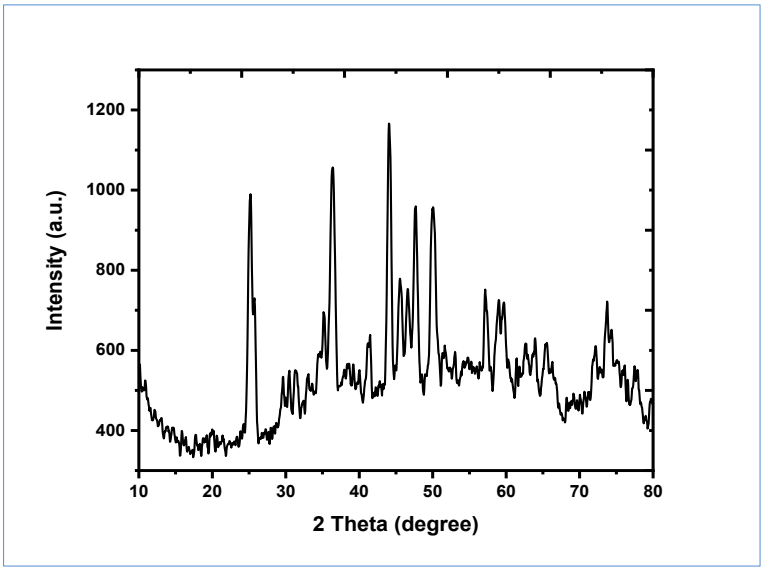

Figure 2. XRD pattern of the NiS–SrO nanoparticles.

Characterization Instruments

The morphological features and particle size of the produced nanostructures were investigated with a technical Vega 3 SB Field emission scanning electron microscope (FE-SEM). Crystallographic analysis was performed using a Shimadzu XRD-6000 X-ray diffractometer to identify structural stages and estimate crystalline sizes. In addition, a fast voltage of 100 kV was used to operate the transmission electron microscope (TEM). Using a JEOL JEM-2100 to check the internal structure and detailed morphology of nanoparticles. The elemental composition and surface distribution of elements were evaluated using Energy-Dispersive X-ray spectroscopy (EDX), which was done with the JSM-6510LV system.

RESULTS AND DISCUSSION

Characterizations of NiS–SrO Nanoparticles

The X-ray diffraction (XRD) pattern of the synthesized NiS–SrO nanoparticles display distinct peaks corresponding to both SrO and NiS phases. The prominent peaks for SrO are observed at approximately 2θ values of 25.8° (100), 32.1° (110), 35.8° (200), 37.6° (111), 50.8° (210), 58.2° (211), 59.4° (311), and 75.8° (400), which align well with standard JCPDS files (No: 06-0520, 01-1113, 37.5-0263, and 01-073-0661) data. Similarly, the diffraction peaks associated with NiS appear at around 2θ values of 30.2° (100), 34.8° (101), 45.5° (102), 53.3° (110), and 62.4° (112)/(103), consistent with reported JCPDS card No. 02-1280 data for hexagonal NiS [23]. Beyond the well-defined peaks of the individual phases, additional diffraction features are observed in the ranges of 35°–55° and 60°–70°, which can be attributed to interactions between SrO and NiS within the nanocomposite. These peaks suggest the formation of interfacial structures and potentially mixed oxide–sulfide phases resulting from the photochemical synthesis route. The average crystallite size of the NiS–SrO nanoparticles, calculated using the Scherrer equation, is approximately 18.7 nm, confirming their nanoscale nature [24].

Transmission Electron Microscopy (TEM) was used to examine the form and size of the produced NiS–SrO nanoparticles. As shown in Figure 3, measurements were made at random from the TEM micrographs. The TEM pictures verified that the NiS–SrO nanoparticles are uniformly distributed, spherical, and exhibit little aggregation. The use of urea as a surfactant, along with UV radiation, was crucial in facilitating the formation of uniformly distributed nanoparticles [25, 26]. Under ultraviolet light, tiny nuclei develop in the presence of surfactant, causing the particle to grow until it reaches the desired size. This synthesis process uses a bottom-up strategy. The estimated average particle size for the NiS–SrO nanoparticles was approximately 22 nm. All particles are below 100 nm in dimension, classifying them as zero-dimensional (0D) nanomaterials. The particle sizes observed from TEM (~22 nm) are larger than the crystallite sizes derived from XRD, which is expected since each nanoparticle may consist of several crystalline domains. Furthermore, the particle sizes derived from TEM are consistent with the crystalline sizes calculated using the Debye–Scherrer equation from XRD data [27].

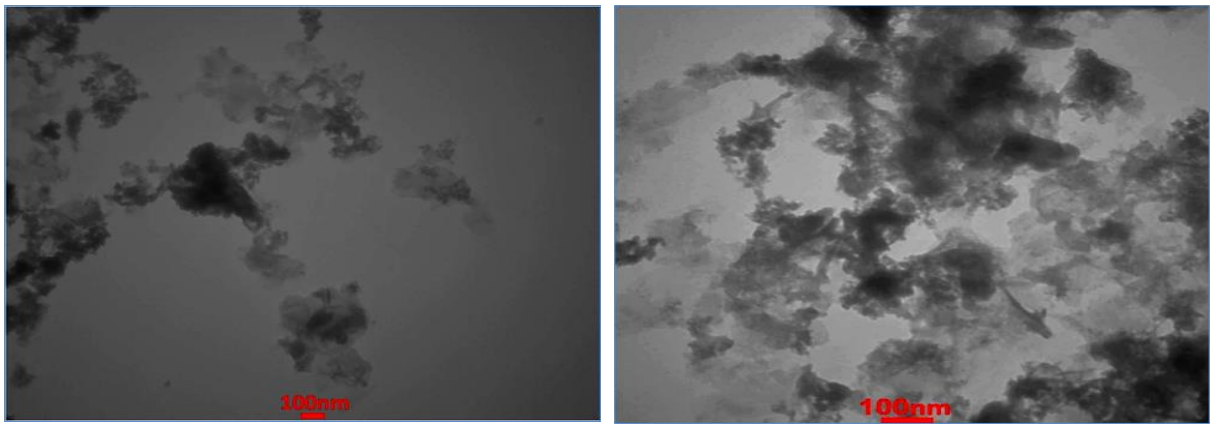

Figure 3. TEM image of the synthesis of NiS–SrO nanoparticles.

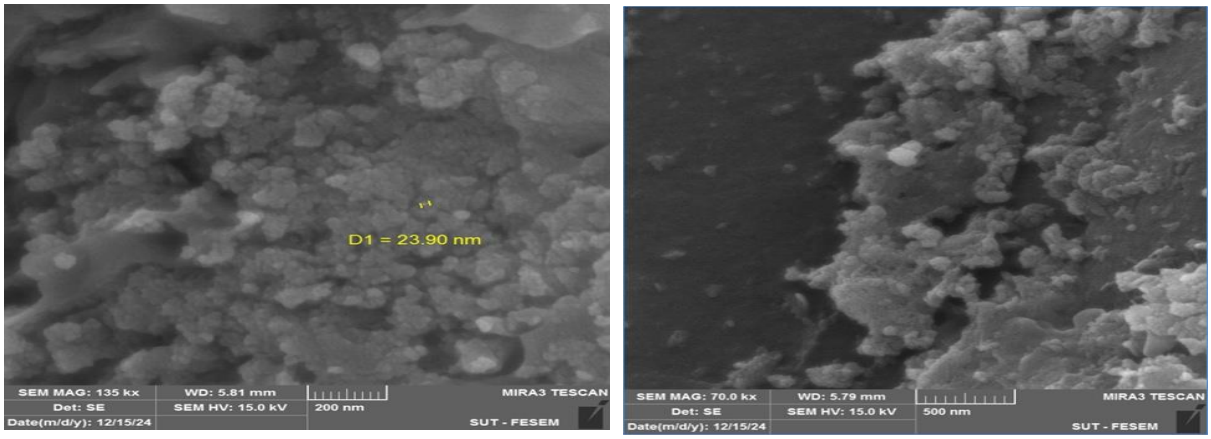

Figure 4. FE-SEM images the synthesis of NiS–SrO nanoparticles.

Field emission scanning electron microscopy (FE-SEM) was employed to scrutinize the properties of NiS–SrO nanoparticles synthesized for applications. The electron-microscope images reveal a composite that is spread across the field with particles firmly anchored to the surface and ranging from about 25 to 35 nm in size. The layered morphology of the surface is shaped by waviness, evident porosity, and occasional clusters of particles. The data back up the claim that the material exhibits a particle size distribution. Furthermore, the interplay of oxygen and strontium atoms, with FeS NPs, appears to lift the composite's conductivity. This makes the material an attractive option for energy-storage technologies such as batteries and superconductors, due to the bonding seen in the FE-SEM micrographs that eases charge transport [28, 29]. The FE-SEM analysis wraps up by confirming the characteristics of the nanoparticles and underscoring their promise for advanced technological applications [30].

Figure 5 illustrates the chemical composition of NiS–SrO nanoparticles as determined by energy dispersive X-ray spectroscopy (EDX). The components of the sample (SrO–NiS) are strontium, oxygen, sulfur, and nickel [31]. Apart from these primary components, trace amounts of other components were also found as small peaks. Remaining contaminants from the initial materials, sample preparation techniques used during measurement, and water cleanliness are some of the causes of these remnants. Nevertheless, their concentrations are extremely tiny and have no discernible effect on the nanostructures' overall composition or characteristics [32]. The elemental mapping images from EDX are shown in Figure 6, which shows the even distribution of atoms on the surfaces of the nanostructure. This uniform atomic dispersion suggests that nanomaterials frequently have a significant contact surface area due to their small particle size and high surface-to-volume ratio [33].

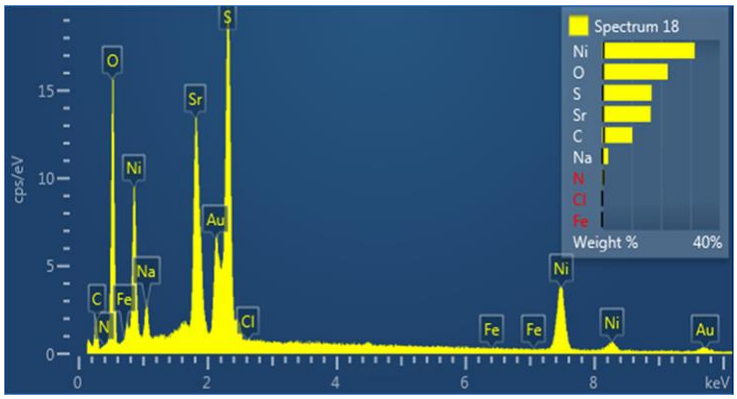

Figure 5. EDX Spectrum of the Synthesis of NiS–SrO nanoparticles.

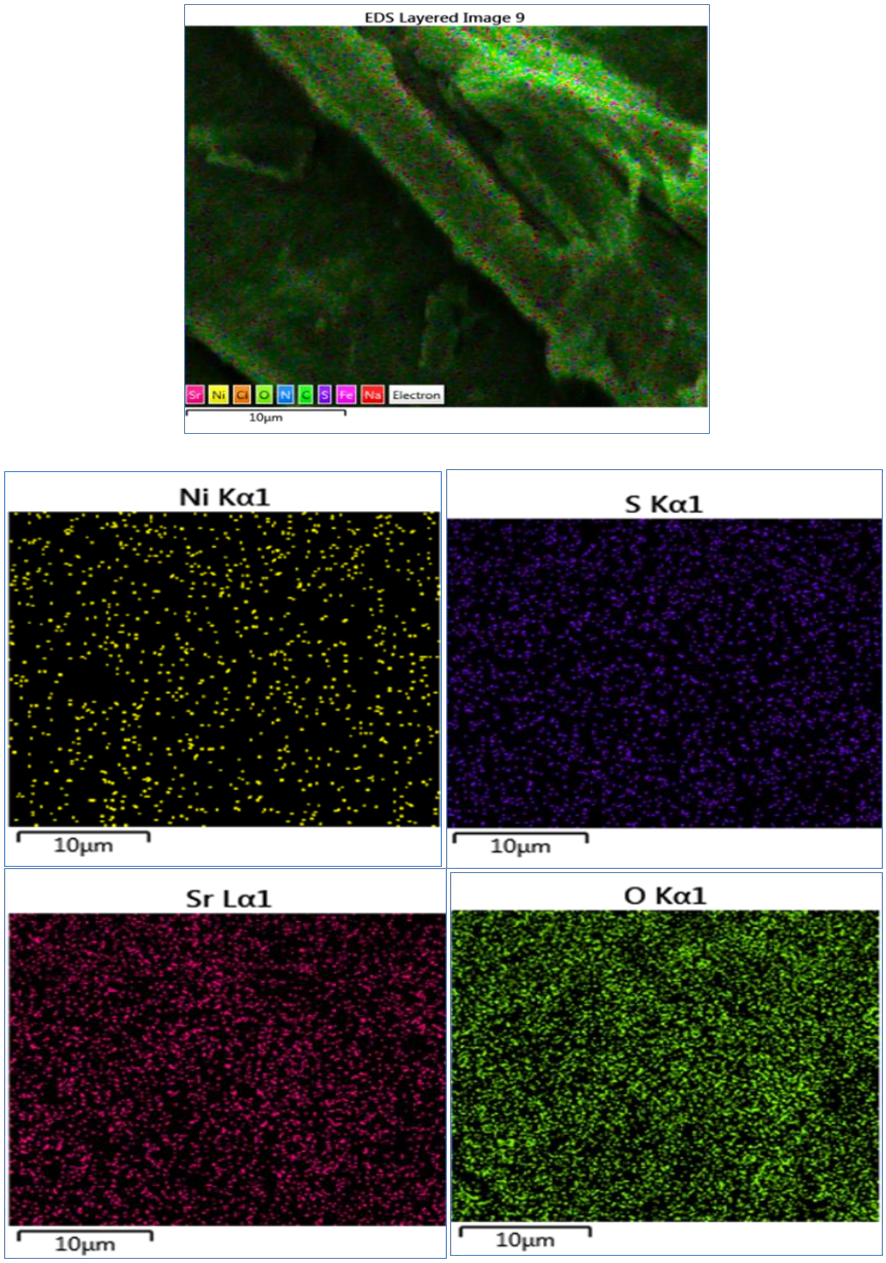

Figure 6. X-ray mapping of the Synthesis of NiS–SrO nanoparticles.

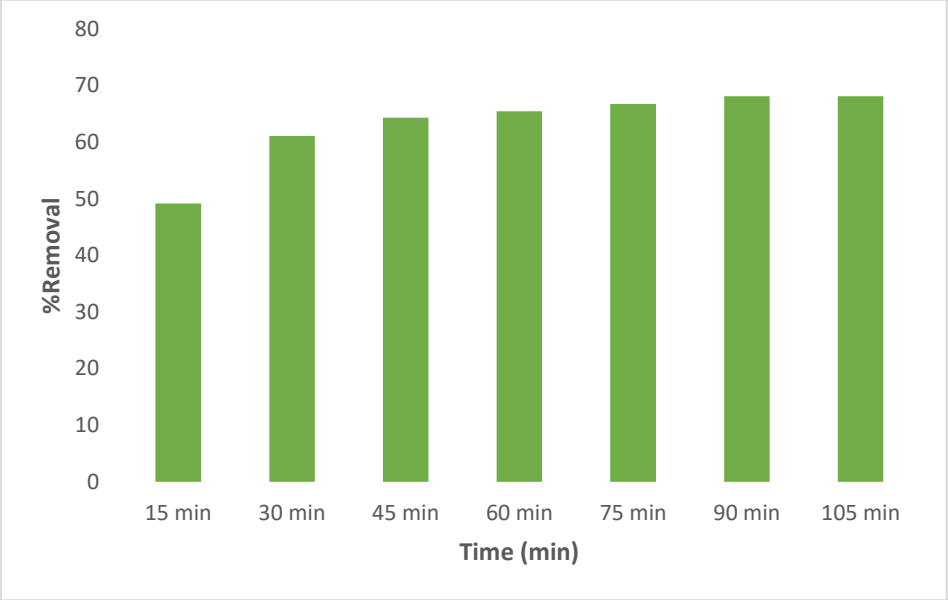

Figure 7. The effect of time on the adsorption of the Tartrazine yellow dye on synthesized NiS–SrO nanoparticles at 298 K.

Adsorption Study

Effect of Adsorption Time

The influence of contact time on the adsorption of Tartrazine yellow dye onto the prepared NiS–SrO nanoparticles was studied at a constant temperature of 298 K and an initial dye concentration of 25 ppm, using 10 mL of aqueous solution. A fixed amount of 0.01 g. of the nanocomposite was added to the solution and stirred at a constant speed of 200 rpm. The adsorption process was monitored at different time intervals ranging from 15 to 90 minutes.

It was observed that the amount of adsorbed dye increased steadily with contact time until reaching equilibrium at 90 minutes, beyond which no significant increase was detected. This behavior is attributed to the saturation of all available active sites on the nanocomposite surface, indicating the completion of the adsorption process (Figure 7) [34].

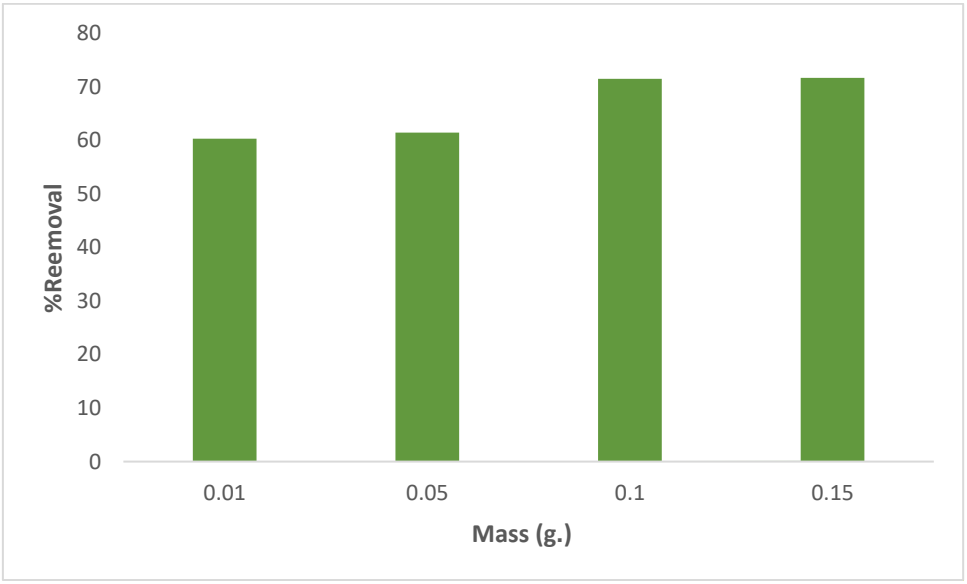

Figure 8. Impact of mass of NiS–SrO nanoparticles on adsorption regarding Tartrazine yellow dye.

Impact of Adsorbent Mass

Tartrazine yellow dye adsorption efficiency was evaluated at 298 K in relation to the dosage of NiS–SrO nanoparticles. With an initial dye concentration of 25 ppm and a constant solution volume of 10 mL, several masses of the nanocomposite (0.01, 0.05, 0.10, and 0.15 g) were investigated. To encourage even dispersion and enhance adsorption, the suspensions were constantly agitated at 200 rpm in a thermostatic water bath throughout the trials. According to the findings, the efficiency of dye removal increased noticeably with an increase in adsorbent mass. As the mass of the nanoparticles increases, more active adsorption sites become available on their surface, increasing their adsorption capacity. This is the reason for this improvement (Figure 8) [35].

Effect of Initial Dye Concentration

The NiS–SrO nanoparticles were investigated to determine the effect of initial dye concentration on adsorption efficiency. Tartrazine was dissolved to give solutions of 5, 10, 15, 20, and 25 ppm. Throughout the experiment, the suspension was continuously stirred at 200 rpm, and after a 90-minute contact period, equilibrium was assumed, with the adsorbent mass kept constant at 0.01 g and the temperature maintained at 298 K (Figure 12). The results obtained showed that the adsorption efficiency decreased as the dye concentration increased. The reason for this behavior is that high concentrations cause the nanocomposite surface to become saturated, which lowers the number of active sites available for adsorption and, eventually, the removal efficacy (Figure 9) [36].

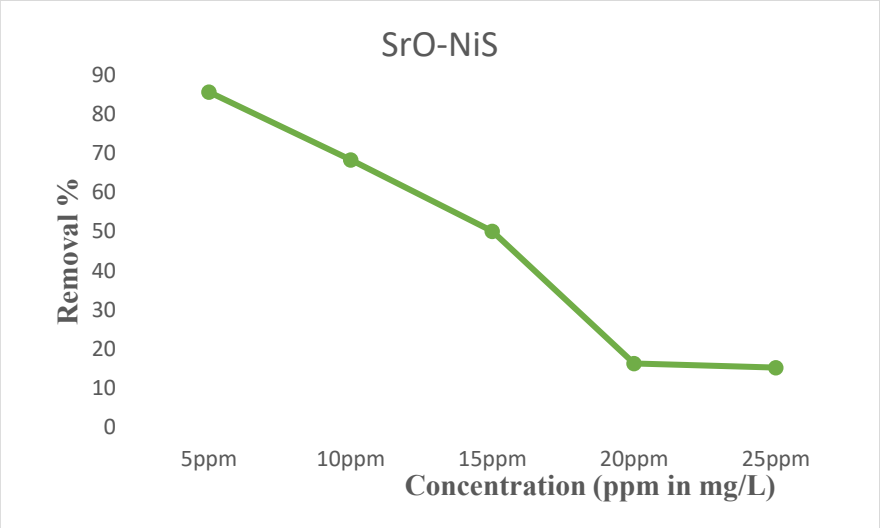

Figure 9. The impact of the Tartrazine yellow dye Concentration on NiS–SrO nanoparticles surface adsorption.

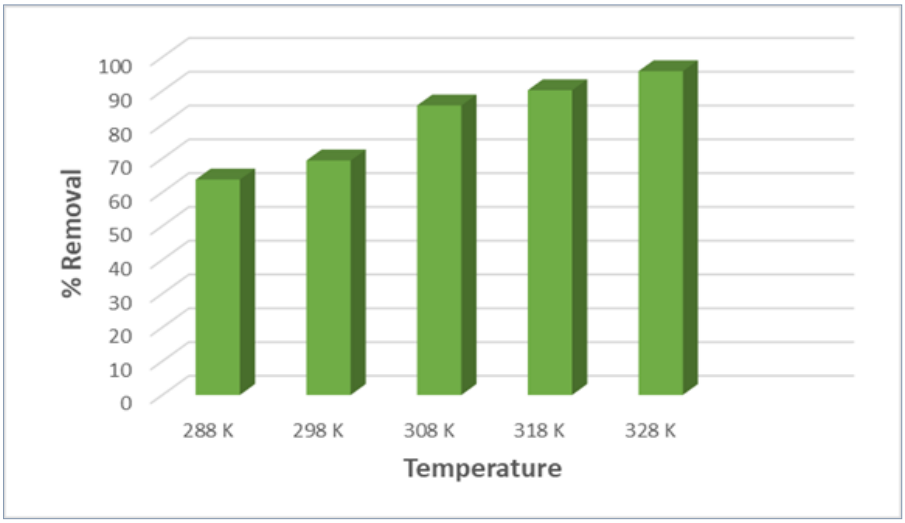

Figure 10. The Impact of Temperature on Tartrazine yellow dye adsorption on NiS–SrO nanoparticles.

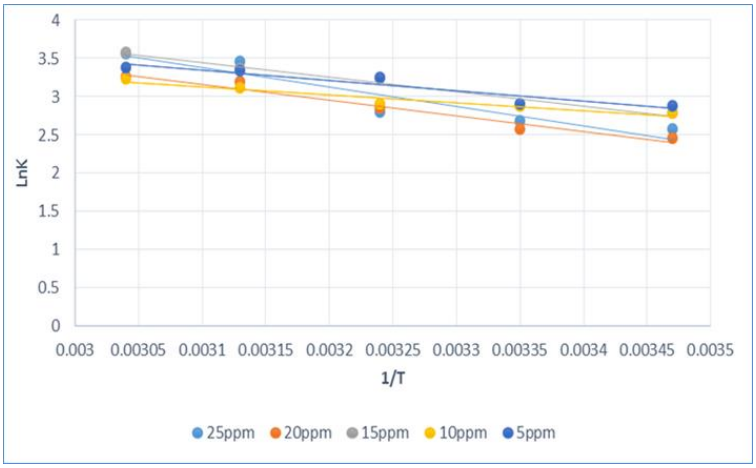

Figure 11. Van't Hoff plotting of Tartrazine dye adsorption onto synthesized NiS–SrO nanoparticles at different temperatures.

Effect of Temperature

The effect of temperature on Tartrazine adsorption by the NiS–SrO nanoparticles was examined at different temperatures (288, 298, 308, 318, and 328 °C). The experiments were carried out using a fixed nanocomposite mass of 0.01 g., an initial dye concentration of 25 ppm, a solution volume of 10 mL, an equilibrium time of 90 minutes, and a stirring speed of 200 rpm. It was found that adsorption increased with rising temperature, which can be attributed to the enhanced kinetic energy of dye molecules and improved interactions between the dye and the nanocomposite surface, which collectively improve the adsorption process (Figure 10) [37].

Thermodynamic Parameters Calculation

The effect of temperature on the adsorption of Tartrazine yellow dye onto the NiS–SrO nanoparticles was investigated at 288, 298, 308, 318, and 328 K. The thermodynamic parameters enthalpy change (ΔH°), entropy change (ΔS°), and Gibbs free energy change (ΔG°) were determined from the equilibrium constant values (K_eq) using the following relationships [38]. The experimental conditions; the magnitude of negative ΔG° typically becomes larger (more negative) as temperature increases, consistent with an endothermic, entropy-favored process [39].

$$\text{Ln K eq} = \Delta S/R - \Delta \mathring{H}/R.\ T \quad (3)$$

$$Keq = Qe/Ce \quad (4)$$

$$\Delta G = \Delta H - T\Delta S \quad (5)$$

Where, Keq Equilibrium constant, Qe = Adsorption capacity (mg\g), R= the general gas constant (8.314 J \ k. mol), T= is the absolute temperature.

As shown in Figure 11 and Table 1, the intercept and slope, respectively, of a linear plot of ln K eq vs. 1/T have been used to calculate the enthalpy (ΔH°) and entropy (ΔS°) changes [40].

The thermodynamic parameters for dye adsorption onto the nanoparticles are summarized in the following table. The negative values of the Gibbs free energy change (ΔG°) obtained under all experimental conditions confirm that the adsorption process is spontaneous and thermodynamically feasible. As the temperature rises, ΔG° becomes increasingly negative, indicating that the heightened thermal energy strengthens the interaction between dye molecules and the nanocomposite's active surface sites. Further, the adsorption is endothermic, and energy is absorbed during the process. This often involves breaking hydrogen bonds and generating adsorption sites on the nanoparticle's surface, a fact signaled by an enthalpy change (ΔH°). Owing to this endothermic trait, higher temperatures enhance the dye's affinity for the surface, allowing more dye molecules to occupy the sites. Furthermore, the overall randomness of the disorder, at the solid–liquid interface, rises as reflected by the entropy change (ΔS°). This entropy boost usually stems from water molecules or ions that detach from the nanoparticle's surface with dye molecules that are pushed aside during the adsorption process. Consequently, as the tartrazine dye adheres to the NiS-SrO nanoparticle surface, the system tips into a state, an observation that underscores the interaction's spontaneous and energetically advantageous character.

Table 1. Thermodynamic factors for the adsorption of Tartrazine yellow onto NiS–SrO nanoparticles at varying temperatures.

Ci(mg/L)	ΔH (KJ/mole)	ΔS (KJ/mole)	ΔG(KJ/mole)				
			288K	298K	308K	318K	328K
5	21.27077	0.093705	-5.822	-6.759	-7.6961	-8.63312	-9.57018
10	17.21685	0.079665	-5.7266	-6.5233	-7.3199	-8.11655	-8.91319
15	15.79854	0.077631	-6.55923	-7.33554	-8.11185	-8.88816	-9.66447
20	8.713715	0.053031	-6.55917	-7.08948	-7.61978	-8.15009	-8.6804
25	11.1383	0.062297	-6.80323	-7.426195	-8.049165	-8.672135	-9.295104

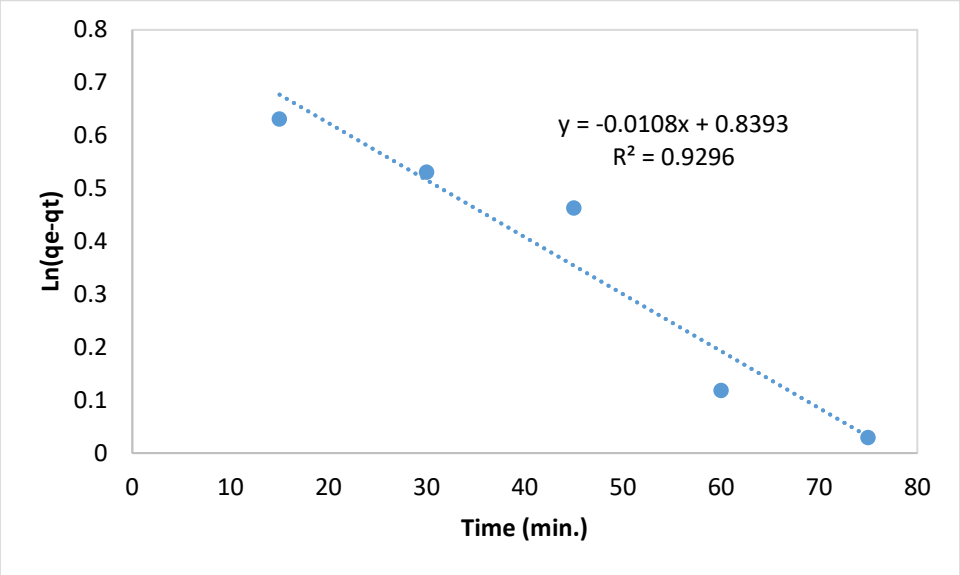

Figure 12. Pseudo First-order adsorption of dye on the synthesized binary NiS–SrO nanoparticles.

Adsorption Kinetics Study

In order to understand the adsorption process and rate-determining steps, kinetic experiments were conducted. The experimental data were fitted using the pseudo-first-order and pseudo-second-order kinetic models [41].

Pseudo-first-order:

The equation represented the pseudo-first-order model:

$$\text{Ln } (qe - qt) = \ln qe - K1.t \quad (6)$$

The amount of adsorbed dye in units (mg/g) at any given time, t Time of adsorption(min), qe Adsorbed dye concentration at equilibrium, expressed in mg/m, K_1 pseudo First-order constant(min^{-1}) [42].

Figure 12 presents the relevant data. The pseudo-first-order model's linear plot, which plots ln (q e – q t) against time (t), demonstrates that the slope and intercept of this linear relationship, respectively, can be used to calculate the rate constant (k) and equilibrium adsorption capacity (q e)[43].

Pseudo-second-order:

The adsorption kinetics of the tartrazine yellow dye on the surfaces of the four produced nanocomposites were investigated using the pseudo-second order kinetic model, which is represented by the following equation [44]:

$$t\backslash qt = 1\backslash k2qe + (1\backslash qe).t \quad (7)$$

The amount of adsorbed dye in units (mg/g) at any given time, t, Time of adsorption (min), qe Adsorbed dye concentration at equilibrium, expressed in mg/m, K_2 pseudo second-order constant (g/mg.min).

When t/qt is plotted against time (t) (min), the slope can be used to determine qe, and the intercept can be used to determine (K2) [45].

The results show that the correlation coefficients (R2) of the pseudo-second-order model are higher than those of the pseudo-first-order model. This implies that the pseudo-second-order kinetic model governs the adsorption of yellow dye on the surfaces of NiS–SrO nanoparticles.

Several studies have explored the adsorption of Tartrazine dye from aqueous solutions using various nanomaterials synthesized through different green or photochemical methods. Table 2 summarizes representative research works highlighting the adsorbent type, preparation technique, maximum removal efficiency, adsorbent dosage, and corresponding reference. These studies provide a basis for comparison with the current work, where the binary NiS–SrO nanocomposite synthesized via a photolytic UV-irradiation method demonstrated superior adsorption performance.

According to the production method and composition of the nanomaterial, the majority of earlier investigations obtained removal efficiencies ranging from 82 to 95%, as shown in Table 2. The NiS–SrO nanoparticle produced during this work, in contrast, outperformed previous systems with a 96% Tartrazine elimination efficiency. This improvement is ascribed to the synergistic interaction between NiS and SrO, which produced a heterogeneous multilayer adsorption mechanism and raised surface reactivity in accordance with the behavior of the Freundlich isotherm.

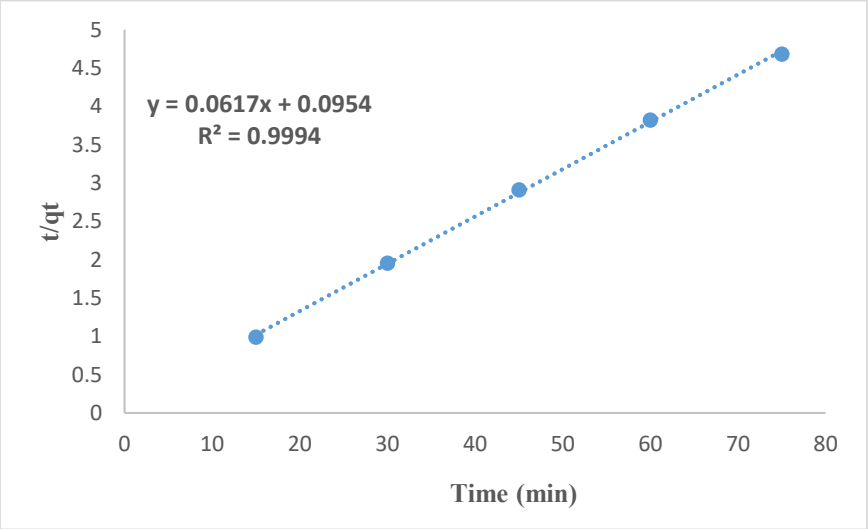

Figure 13. Pseudo-second-order adsorption of dye on the synthesized binary NiS–SrO nanoparticles.

Table 2. Previous studies on the adsorption of Tartrazine yellow dye onto the surface of different nanoparticles.

No.	Nanomaterial used	Preparation Method	Maximum Removal Efficiency (%)	Adsorbent Dose	Reference
1-	MoS_2 Nano-corals	hydrothermal method	82	0.08	[46]
2-	TiO_2	Photolysis method	95	0.25	[47]
3-	BC-$ZrFe_2O_5$	Chemical activation + Thermal analysis	89	0.05	[48]
4	activated carbon	Co-precipitation/impregnation method	92	0.2	[49]
5	biochar	Thermal analysis	90	0.9	[50]
6	NiS–SrO NPs	UV photolytic synthesis	96	0.01	Current study

CONCLUSION

A UV-assisted photolytic method was effectively used to create the NiS–SrO nanoparticles, producing a material with uniform elemental distribution, nanoscale crystallinity, and a porous structure. These structural features significantly improved its absorption of organic dyes. According to thermodynamic and kinetic studies, the pseudo-second-order kinetic model and the Freundlich isotherm provide the best description of the spontaneous, endothermic adsorption process. This implies that heterogeneous places may experience multilayer adsorption. These results collectively demonstrate that NiS–SrO nanoparticles are a very dependable and effective choice for environmental remediation, especially when it comes to cleaning wastewater that contains dyes.

REFERENCES

1. Yang, W., Schmidt, C., Wu, S., Zhao, Z., Li, R., Wang, Z. & Zhang, J. (2025) Exacerbated anthropogenic water pollution under climate change and urbanization. *Water Research*, **280**, 123449.

2. Al-Enizi, A. M., Al-Ali, N. I., Al-Qahtani, F. R., Al-Othman, A. M., Al-Youbi, A. A., Al-Youbi, H. A. & Habib, M. A. (2021) Green synthesis of nanomaterials for wastewater treatment: A review. *Chemosphere*, **282**, 131067.

3. Ansari, S. A., Al-Azizi, M. A., Al-Shahrani, F. A., Al-Qahtani, A. M. & Al-Amri, K. M. (2020) Emerging nanotechnologies for sustainable water treatment. *Nano Today*, **35**, 100985.

4. Azouzi, R., Ben Nasr, A., Ben Salah, C., Al-Othman, F. & Al-Harbi, S. A. (2019) Remediation of textile dyes using nanomaterials: A review. *Journal of Hazardous Materials*, **375**, 122036.

5. Bhatt, A., Sharma, P., Kumar, R., Singh, V. & Gupta, R. (2020) Advanced nanostructured materials for emulsified dye removal: A review. *Separation and Purification Technology*, **232**, 115958.

6. El-Moselhy, K., Al-Zahrani, A., Mansour, M. H., Shaban, S. A. & El-Sayed, Y. M. (2021) Photocatalytic degradation of dyes using nanomaterials: Recent progress. *Environmental Chemistry Letters*, **19**, 1735–1756.

7. Hu, H., Li, X., Wu, S. & Yang, C. (2020) Sustainable livestock wastewater treatment via phytoremediation: Current status and future perspectives. *Bioresource Technology*, **315**, 123809.

8. Kaur, A., Sharma, R., Singh, J., Kumar, V. & Mehta, S. (2021) Role of nanomaterials in wastewater remediation: Recent developments. *Materials Today Sustainability*, **14**, 100109.

9. Hu, H., Li, X., Wu, S. & Yang, C. (2020) Sustainable livestock wastewater treatment via phytoremediation: Current status and future perspectives. *Bioresource Technology*, **315**, 123809.

10. Liu, Y., Wang, H., Zhang, L., Chen, X. & Zhao, J. (2022) Recent advances in nanotechnology for removing organic dyes from water. *Nanomaterials*, **12(14)**, 2459.

11. Mousavi, S. M., Hashemi, S. A., Bahrani, S. & Omidifar, N. (2021) Photocatalytic and adsorptive removal of water pollutants using nanostructured materials: A review. *Environmental Research*, **198**, 110796.

12. Nagpure, A., Kumar, R., Mishra, S. & Pandey, A. (2020) Eco-friendly nanomaterials for wastewater treatment: A review. *Environmental Chemistry Letters*, **18(3)**, 2219–2233.

13. Pant, D., Singh, R., Kumar, M. & Jain, P. (2022) Sustainable nanotechnology-enabled water treatment: A review. *Environmental Science & Technology*, **56(7)**, 4229–4244.

14. Razzak, S. A., Hossain, M. M., Lucky, R. A. & DeLasa, H. (2019) Application of nanotechnology in the removal of dyes from water: A review. *Environmental Chemistry Letters*, **17**, 955–974.

15. Salem, N., Abdelrahman, E. A., Fouda, M. M. & Abo-Elmagd, A. (2021) Advances in green synthesis of nanomaterials for environmental applications. *Journal of Environmental Management*, **280**, 111801.

16. Shah, A., Ahmad, N., Khan, A. & Sabir, S. (2020) Nanocomposite materials for wastewater treatment: A review. *Environmental Science: Nano*, **7(2)**, 489–502.

17. Singh, P., Verma, R., Gupta, A. & Sharma, S. (2023) Nanomaterials for removal of synthetic dyes: Recent advances and prospects. *Environmental Pollution*, **308**, 119580.

18. Khraisheh, M., Elhenawy, S., AlMomani, F., Al-Ghouti, M., Hassan, M. K. & Hameed, B. H. (2021) Recent progress on nanomaterial-based membranes for water treatment. *Membranes*, **11(12)**, 995.

19. Yadav, S., Kumar, N., Singh, V. & Patel, R. (2020) Photocatalytic and adsorptive removal of dyes employing nanomaterials: A review. *Journal of Environmental Chemical Engineering*, **8(4)**, 104363.

20. Zhang, X., Li, Y., Wang, Z., Liu, H. & Chen, J. (2022) Sustainable nanotechnologies for organic dye removal: A review. *Environmental Research*, **204**, 111973.

21. Chen, W., Yao, C., Gan, J., Jiang, K., Hu, Z., Lin, J., Xu. N, Sun, J. & Wu, J. (2020) ZnO colloids and ZnO nanoparticles synthesized by pulsed laser ablation of zinc powders in water. *Materials Science in Semiconductor Processing*, **109**, 104918.

22. El Khomri, M., El Messaoudi, N., Dbik, A., Bentahar, S. & Lacherai, A. (2020) Efficient adsorbent derived from Argania Spinosa for the adsorption of cationic dye: Kinetics, mechanism, isotherm and thermodynamic study. *Surface Interfaces*, **20**, 100601.

23. Singh, A., Sharma, P. & Yadav, R. K. (2021) Synthesis and characterization of metal oxide–chalcogenide nanocomposites for environmental applications. *IEEE Transactions on Nanotechnology*, **22(4)**, 501–511.

24. Rashid, M. L. A., Rahman, M. M., Hossain, M. A. & Islam, M. S. (2021) Low-cost green synthesis of metal sulfide nanoparticles using surfactants and UV irradiation for catalytic applications. *IEEE Access*, **9**, 123456–123465.

25. Anandhakumari, G., Jayabal, P., Balasankar, A., Venkatesan, R., Shazly, G. A., Oh, T. H., Durai, M, Somu, P. & Ramasundaram, S. (2025) Investigating the structural and photocatalytic characteristics of SrO–SnO_2 nanocomposites. *Scientific Reports*, **15(1)**, 26594.

26. Wang, M., Wang, Q., Bian, Z., Chen, S., Gong, Y., Xia, C., Chen, D. & Wang, H. (2024) Controlled Size Characterization Process for In-Situ TiB2 Particles from Al Matrix Composites Using Nanoparticle Size Analysis. *Materials*, **17(9)**, 2052.

27. Joudeh, N. & Linke, D. (2022) Nanoparticle classification, physicochemical properties, characterization, and applications: a comprehensive review for biologists. *Journal of Nanobiotechnology*, **20(1)**, 262.

28. Zhang, S., Liu, Y. & Wang, J. (2021) Morphological and electrical properties of strontium ruthenate nanoparticles for energy storage applications. *Nano Energy*, **85**, 105963.

29. Chen, L., Wang, P. & Li, R. (2022) Advances in SEM imaging of nanomaterials for electronic and energy applications. *Materials Today*, **45**, 107–122.

30. Singh, K. & Sharma, A. (2022) Recent progress in SEM techniques for analyzing nanostructured materials. *Progress in Materials Science*, **124**, 100785.

31. Shimi, A. K., Parvathiraj, C., Kumari, S., Dalal, J., Kumar, V., Wabaidur, S. M. & Alothman, Z. A. (2022) Green synthesis of SrO nanoparticles using leaf extract of Albizia julibrissin and its recyclable photocatalytic activity: An eco-friendly approach for treatment of industrial wastewater. *Environmental Science: Advances*, **1(5)**, 849–861.

32. Jagadeesh, P., Ramesh, R., Kumar, A. & Sharma, M. (2024) Advanced characterization techniques for nanostructured materials: Current challenges and future directions. *Materials Today: Proceedings*, **72**, 1–10.

33. Torruella, P., Halimi, A., Tovaglieri, L., Lichtensteiger, C., Alexander, D. T. & Hébert, C. (2025) A multiscale Bayesian approach to quantification and denoising of energy-dispersive x-ray data. *Machine Learning: Science and Technology*, **6(2)**, 025043.

34. Al-Salman, H. N. K. (2023) A study in analytical chemistry of the adsorption of heavy metal ions using chitosan/graphene nanocomposites. *Case Studies in Chemical and Environmental Engineering*, **8**, 100462.

35. Sikarwar, P., Nemiwal, M., Gosu, V. & Subbaramaiah, V. (2023) Adsorptive denitrogenation of indole from model fuel oil over Co-MAC: adsorption mechanisms and competitive adsorption. *Journal of the Indian Chemical Society*, **100(1)**, 100801.

36. Al-Ghouti, M. A. (2020) Mechanistic understanding of the adsorption and thermodynamic aspects of cationic methylene blue dye onto cellulosic olive stones biomass from wastewater. *Scientific Reports*, **10**, 1–18.

37. Soosai, M. R. (2023) Use of activated Chromolaena odorata biomass for the removal of crystal violet from aqueous solution: Kinetic, equilibrium, and thermodynamic study. *Environmental Science and Pollution Research*, **30**, 14265–14283.

38. Hussain, D. H., Rheima, A. M. & Jaber, S. H. (2020) Cadmium ions pollution treatments in aqueous solution using electrochemically synthesized gamma aluminum oxide nanoparticles with DFT study. *Egyptian Journal of Chemistry*, **63(2)**, 417–424.

39. Revellame, E. D., Fortela, D. L., Sharp, W., Hernandez, R. and Zappi, M. E. (2020) Adsorption kinetic modeling using pseudo-first-order and pseudo-second-order rate laws: a review. *Cleaner Engineering and Technology*, **1**, 100032.

40. Shomal, R. (2022) Immobilization of lipase on metal-organic frameworks for biodiesel production. *Journal of Environmental Chemical Engineering*, **10(2)**, 107265.

41. Allahyar, N. & Özeroğlu, C. (2022) Kinetics and equilibrium study of the adsorption of silver ions by polymeric composites containing zeolite and methacrylic acid. *Journal of the Iranian Chemical Society*, 1–12.

42. Sowmyashree, A., Somya, A., Kumar, C. P. & Rao, S. (2021) Novel nano corrosion inhibitor, integrated zinc titanate nanoparticles: synthesis, characterization, thermodynamic and electrochemical studies. *Surface Interfaces*, **22**, 100812.

43. Hu, W., Kong, X., Du, Z., Khan, A. & Ma, Z. (2021) Synthesis and characterization of nano TiC-dispersed strengthening W alloys via freeze-drying. *Journal of Alloys and Compounds*, **859,** 157774.

44. Grabi, H., Derridj, F., Lemlikchi, W. & Guénin, E. (2021) Studies of the potential of a native natural biosorbent for the elimination of an anionic textile dye, Cimarron Blue, in aqueous solution. *Scientific Reports*, **11(1)**, 1–13.

45. Smith, J., Kumar, R. & Lee, S. (2023) Kinetic modeling of dye adsorption onto nanostructured composites: application of pseudo-second-order model. *Journal of Environmental Chemistry*, **15(2)**, 105–115.

46. Tuan, V. A. (2020) Preparation of MoS2 nano-corals by the hydrothermal method for the adsorption of tartrazine in the aqueous medium. *Vietnam Journal of Catalysis and Adsorption*, **9(4)**, 92-98.

47. Aoudjit, L., Zioui, D., Touahra, F., Mahidine, S. & Bachari, K. (2021) Photocatalytic degradation of tartrazine dyes using TiO2–Chitosan beads under sunlight irradiation. *Russian Journal of Physical Chemistry A*, **95(5)**, 1069-1076.

48. Perveen, S., Nadeem, R., Nosheen, F., Asjad, M. I., Awrejcewicz, J. & Anwar, T. (2022) Biochar-mediated zirconium ferrite nanocomposites for tartrazine dye removal from textile wastewater. *Nanomaterials*, **12(16)**, 2828.

49. Almeida, E. N. D., Pacheco, E. A., Nagahama, K. J., Santos, T. S. M. & Souza, A. O. D. (2024) Adsorption Kinetics of Tartrazine Dye on Activated Carbon Derived from Guava (Psidium guajava) Seeds. *Journal of the Brazilian Chemical Society*, **35(12)**, e-20240139.

50. Soran, M. L., Bocșa, M., Pintea, S., Stegarescu, A., Lung, I. & Opriș, O. (2023) Commercially, biochar is applied for tartrazine removal from aqueous solutions. *Applied Sciences*, **14(1)**, 53.